Au and Pt remain unoxidized on CeO_2 based catalyst during WGS reaction

Tomas R. Reina[1,2*], Miriam Gonzalez-Castaño[1*], Victor López-Flores[1,3], L. Marcela Martínez T.[1] , Andrea Zitolo[3], S. Ivanova[1], Wenquian Xu[4] , Miguel Angel Centeno[1], Jose Antonio Rodriguez[4] and Jose Antonio Odriozola[1,2]

corresponding authors: gonzalez@b-tu.de ; tramirez@us.es; [*]authors share equal contributions as first authors

[1]*Inorganic Chemistry Department and Materials Science Institute, University of Seville-CSIC, 41092 Sevilla, Spain.*

[2]*Department of Chemical and Process Engineering, University of Surrey, Guildford GU2 7XH, UK.*

[3]*Synchrotron SOLEIL, L'Orme des Merisiers, Saint-Aubin, B.P. 48, 91192 Gif-sur-Yvette, France*

[4]*Chemistry Division, Brookhaven National Laboratory, Upton, New York 11973.*

Abstract

The active form of Au and Pt in CeO_2 based catalysts for the WGS reaction is an issue that although it has been widely studied remains unclear. On one hand, ionic species might be responsible of weakening the Ce-O bonds increasing the oxygen mobility and WGS activity. On the other hand, the close contact of Au or Pt atoms with CeO_2 oxygen vacancies at the metal/CeO_2 interface might provide the active sites for an efficient reaction. In this work, by using *in-situ* X-ray absorption spectroscopy, we demonstrate that both Au and Pt remain unoxidized during the reaction. Remarkable differences involving the dynamics established by both species under WGS atmospheres were recognized. For the pre-reduced Pt catalyst, an increase of the conversion coincided with a re-structuration of the Pt atoms into cuboctahedrical metallic particles without significant variations on the overall particle size. Contrary to the relatively static behavior of Pt^0, Au^0 nanoparticles exhibited a sequence of particle splitting and agglomeration whilst maintaining a zero oxidation state, even though not being located in a metallic environment during the process. *High WGS activity was obtained when Au atoms were surrounded by oxygen.* The fact that Au preserves its unoxidized state indicates that the chemical interaction between Au and oxygen must be necessarily electrostatic being such electrostatic interaction fundamental for a top performance in the WGS process.

Keywords: *Pt; Au; metal; Water Gas Shift reaction; active phase*

INTRODUCTION

Hydrogen is recognized as one of the most promising future fuels since it is a clean, renewable and highly efficient energy carrier [1]. The purification of H_2 by CO removal processes is one of the major challenges to face in order to definitely deploy a "hydrogen economy" as a real energy alternative [2]. In this respect, an old chemical process as the water gas shift (WGS, $CO + H_2O \rightleftharpoons H_2 + CO_2$) reaction has received a renewed interest and it is under intensive investigation [2–5]. The development of efficient heterogeneous catalysts for this process is inseparably associated to the success of hydrogen-based technologies.

Among the studied catalysts, Pt- and Au-CeO_2 based systems have been broadly employed exhibiting remarkable activity in the WGS [6–8]. In general terms, it is well accepted that CO is absorbed on the metal nanoparticles while H_2O is activated in the oxygen vacancies of the cerium oxide and the subsequent steps proceed on the metal-CeO_2 interface [9,10]. Nevertheless, what it is not so clear is the nature of the catalytically active Au and Pt species. Despite the vast literature behind Au and Pt WGS catalysts this issue remains controversial [11–13]. Flytzani-Stephanopoulos and coworkers have published that the active species of Au and Pt in nanostructured CeO_2 materials are nonmetallic (cationic) species strongly associated with the surface CeO_2 oxygen groups [14,15]. After applying a leaching process, they remove metallic Au species and they ended up with high effective WGS catalysts with a very low amount of noble metal where the active species are $Au^{\delta+}$. They concluded that metallic Au nanoparticles are un-important in the WGS reaction over Au-CeO_2 [15].

Opposite observations have been however reported for both noble metals establishing M^0-O_v-Ce^{3+} as the main WGS active sites [16–18]. Thus, investigations reported by Kim and Thompson contradict the Au cationic as active WGS species [19]. Even though using the same leaching methodology that in ref. [15], the unleached catalysts were much more active that the leached ones [19]. Karpenko *et al.* [20] found that after the leaching process both cationic and metallic Au species remain in the catalysts. Similar disagreements concerning the oxidation state of active Pt species are reported being both PtO_x and Pt^0 species the active phases [21,22]. Namely, studies conducted by Ding et al. [23] on Pt supported catalysts proposed Pt^0 as the WGS active site whilst $Pt^{\delta+}$ species were mere spectators. These results challenge the idea of cationic metal species and situate the active site on unoxidized Au and Pt nanoparticles.

The diversity in author opinions regarding both active species seems to be a never-ending topic. Despite its complexity, this question has to be addressed since it is crucial to understand and design efficient Au and Pt based catalysts for the WGS reaction. In this work, we have shed some light to close the debate. Using *in-situ* XAS experiments on iron-doped Au/ and Pt/ CeO_2 catalysts, the nature of active Au and Pt species has been identified. Despite the fact that only *metallic* Au and Pt particles are present in the whole reaction, during the WGS the close interaction of Au with oxygen from CeO_2 results on an incipient AuO_x formation where Au remains as Au^0. Our observations unifies previous hypotheses demystifying the nature of the active phase in the WGS process.

EXPERIMENTAL

Ceria based supports were prepared over commercial γ-Al_2O_3 (Sasol) by wetness impregnation using their corresponding metal precursors $Ce(NO_3)_4 \cdot 6H_2O$ and $Fe(NO_3)_3 \cdot 9H_2O$ (Aldrich) in order to obtain 15 *wt*.%/CeO_2/Al_2O_3 and 15 *wt*.%$Ce_{0.8}Fe_{0.2}O_2/Al_2O_3$ supports. Once impregnated, the obtained solids were dried and calcined at 450°C for 4h. The obtained supports were labelled CeAl and CeFeAl, respectively. For Au and Pt catalysts, different synthesis methods were employed with the aim of achieving metal content *ca*. 2 *wt*.%. with comparable metal dispersions [24]. Thus, Pt catalysts were synthetized via incipient wetness impregnation using the tetrammonium nitrate platinate solution as Pt precursor slightly modified with acetic acid 1M [25]. Instead, Au catalysts were prepared by direct anionic exchange method using $HAuCl_4$ as Au precursor. The catalysts were calcined at 350°C. Over the three different supports: γ-Al_2O_3, 15 *wt*.%/CeO_2/Al_2O_3 and 15 *wt*.%$Ce_{0.8}Fe_{0.2}O_2/Al_2O_3$, the obtained Pt and Au catalysts were labelled correspondingly, Pt/Al, Au/Al, Pt/CeAl, Au/CeAl, Pt/CeFeAl and Au/CeFeAl. The chemical composition of the prepared catalysts was evaluated by X-ray microfluorescence spectrometry and the measurements were conducted in an EDAX Eagle III spectrophotometer equipped with a Rh cathode. The catalytic activity of the samples was evaluated in a tubular flow reactor at 4000 h^{-1} using feed streams composed by 4.5 *vol*.%CO + 30 *vol*.% H_2O (N_2 balanced). *Operando* XAS spectra were collected on Pt L_3-edge, Au L_3-edge and Ce L_3-edge during the WGS reaction. Details of each experiment are described in the Supplementary Information.

RESULTS

The chemical composition of both noble metals catalysts employed in this study is presented in **Table S1**. Full details of catalysts preparation and characterization can be found elsewhere [24,26].

The catalytic activity of the Pt/ and Au/CeO_2 catalysts for the WGS reaction is depicted in Fig. 1. The graph evidences the impact of the noble metal nature and the role of CeO_2 in the WGS reaction. It is also evident that the support has a deeper influence on Au catalysts than in Pt ones, although it must be noticed that at low temperatures, Au catalysts are always more active than the corresponding Pt ones. Whilst the Pt intrinsic ability for performing water splitting and CO oxidation renders the Pt/Al_2O_3 catalyst an active system for the WGS reaction, Au/Al_2O_3 is hardly active pointing the need of an "active support" like CeO_2 in which oxygen vacancies enable the water activation, which is the controlling reaction step [27]. In view of the later, the creation of oxygen vacancies on CeO_2 is desirable to achieve high catalytic performances. Actually, the oxygen vacancies of CeO_2 play a multirole on the reaction. On one hand, they are the reactive sites for water splitting and on the other hand, they act as preferential nucleation points for metal deposition allowing high metallic dispersion and improving the catalytic performance [28,29].

This interaction O-vacancy/metallic center involves a charge transfer from the structural defects towards noble metal atoms, modulating the activity of the Au and Pt based catalysts [24]. Previous reports demonstrated that the addition of small amounts of iron increases the oxygen vacancies population on CeO_2 based systems resulting in a remarkable activity in the WGS process [18, 22]. Fig. 1 also demonstrates the superiority of the iron doped system which is able to achieve very high CO conversions at 300 ºC. Iron-doped CeO_2 based catalysts can be considered as an interesting approach towards the new generation of WGS catalysts and therefore it was selected to face the main question of this paper: What is the nature of the active Au and Pt species during the WGS?

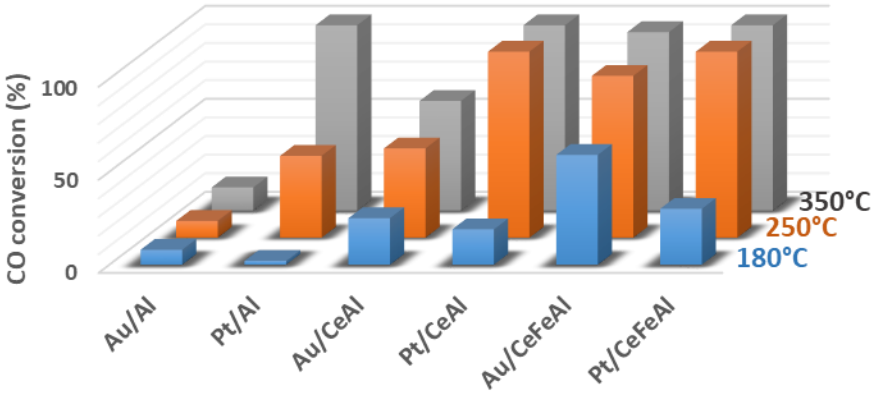

Figure 1. Catalytic activity of Pt and Au supported catalysts (4.5%CO+30%H_2O; 4000 h^{-1})

Fig. 2A and 2B shows Pt-L_3 and Ce-L_3 XANES spectra obtained for the Pt/CeFeAl catalyst during the pre-reduction treatment (not conducted for Au/CeFeAl catalyst). The evolution of the formal oxidation state of Pt and Ce atoms during the pre-reduction treatment are shown in **Table S2**. Before the introduction of H_2, the Pt-L_3 XANES of the Pt/CeFeAl sample (Fig. 2A) shows the characteristic PtO sharp rising absorption peak at 11564 eV underlining the existence of oxidized Pt atoms. This absorption peak, denominated the "white line", directly accounts for the vacancies on 5d orbital when Pt species are oxidized [30]. These PtO_x species are reduced by H_2 starting from room temperatures as indicated by the decrease of the intensity of the white line until a totally reduced Pt state is reached.

The different XANES line shapes characteristic of Ce^{3+} and Ce^{4+} species [19] permitted us to discern the evolution of the Ce-L_3 XANES absorption with the temperature when exposed to H_2 rich streams. At 25 ºC, the Ce-L_3 XANES spectrum show two absorption peaks. The lower energy absorption peak is commonly attributed to the absorption from 2p level to the 5d with the 4f orbital remaining unoccupied, resulting in a Ce $[2p^5 4f^0 5d^1]O[2p^6]$ state configuration [31,32]. The second absorption characteristic of Ce^{4+} appears at higher energies and it is assigned to an electron transfer from the oxygen valence band to the CeO_2 4f shell leaving a hole in the oxygen valence band, with a final $Ce[2p^5 4f^1 5d^1]O[2p^5]$ state configuration [31,32]. The Ce-L_3 XANES spectrum obtained prior the H_2 contact significantly changes when the temperature is increased. Meanwhile, the Ce^{4+} absorption bands intensity decreases, a new peak is observed and related to the appearance of Ce^{3+} species. For the Ce^{3+} species, in which the 4f shell is partially occupied, the observed transition is associated to the absorptions from 2p to 5d, with the initial and final configuration states for the electron transfer corresponding to $Ce[2p^6 4f^1 5d^0]O[2p^6]$ and $Ce[2p^5 4f^1 5d^1]O[2p^6]$ [31,32].

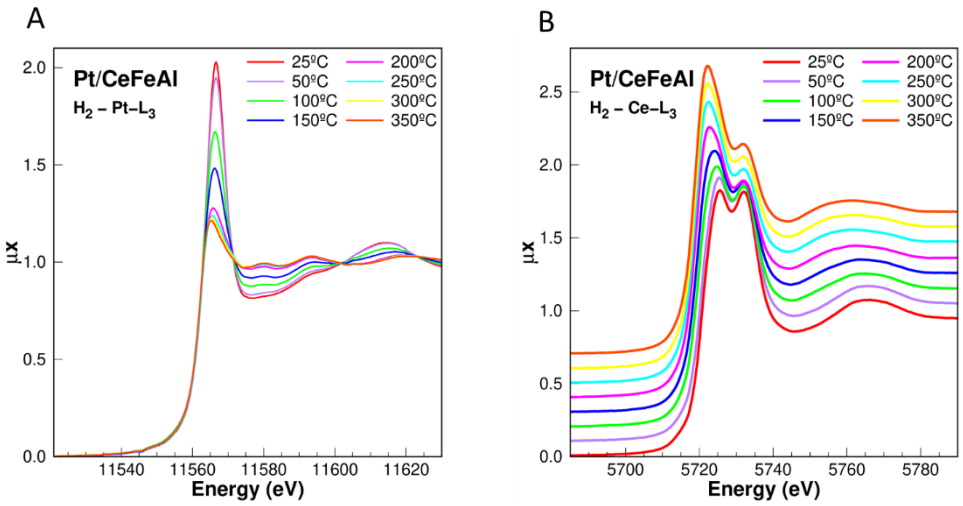

Figure 2. XANES spectra obtained during the H_2 pre-activation treatment for: a) Pt-L_3 absorption edge; b) Ce-L_3 absorption edge

Fig. 3 shows the normalized background subtracted XAS Pt-L_3 and Au-L_3 spectra under WGS atmospheres. For the pre-reduced Pt catalyst, the Pt and Ce formal oxidation state and defects concentration remain almost unchanged whatever the reaction temperature (**Table S3, S4 and S5**, respectively). In agreement with the studies of Ding et al. [23], the XANES data revealed Pt^0 as the major active site in Pt/CeO_2 catalysts under WGS reaction conditions. In a similar way, the Au-L_3 XANES spectra resembled that of the metallic Au for all the studied temperatures. Indeed, no evidence of the white line fingerprints of oxidized metals with partially occupied d-band is noticed [33]. Furthermore, there is no displacement of the absorption edge position towards higher energies that would correspond to an oxidized state. Therefore, it must be concluded that Au remains as Au^0 during the WGS. Contrary to the observations of Flytzani and coworkers [15], in our Au-based sample, Au preserves a formal oxidation state of (0) from the very beginning of the WGS reaction. However, structural changes that take place in the process facilitate the contact between Au and lattice oxygen from CeO_2, resulting in the existence isolated Au atoms surrounded by O. The Au-O contact is in line with the theory of $Au^{\delta+}$ as active goldspecies. Experimental evidences in support of this close Au-O contact are given by the analysis of EXAFS data (Fig. 3).

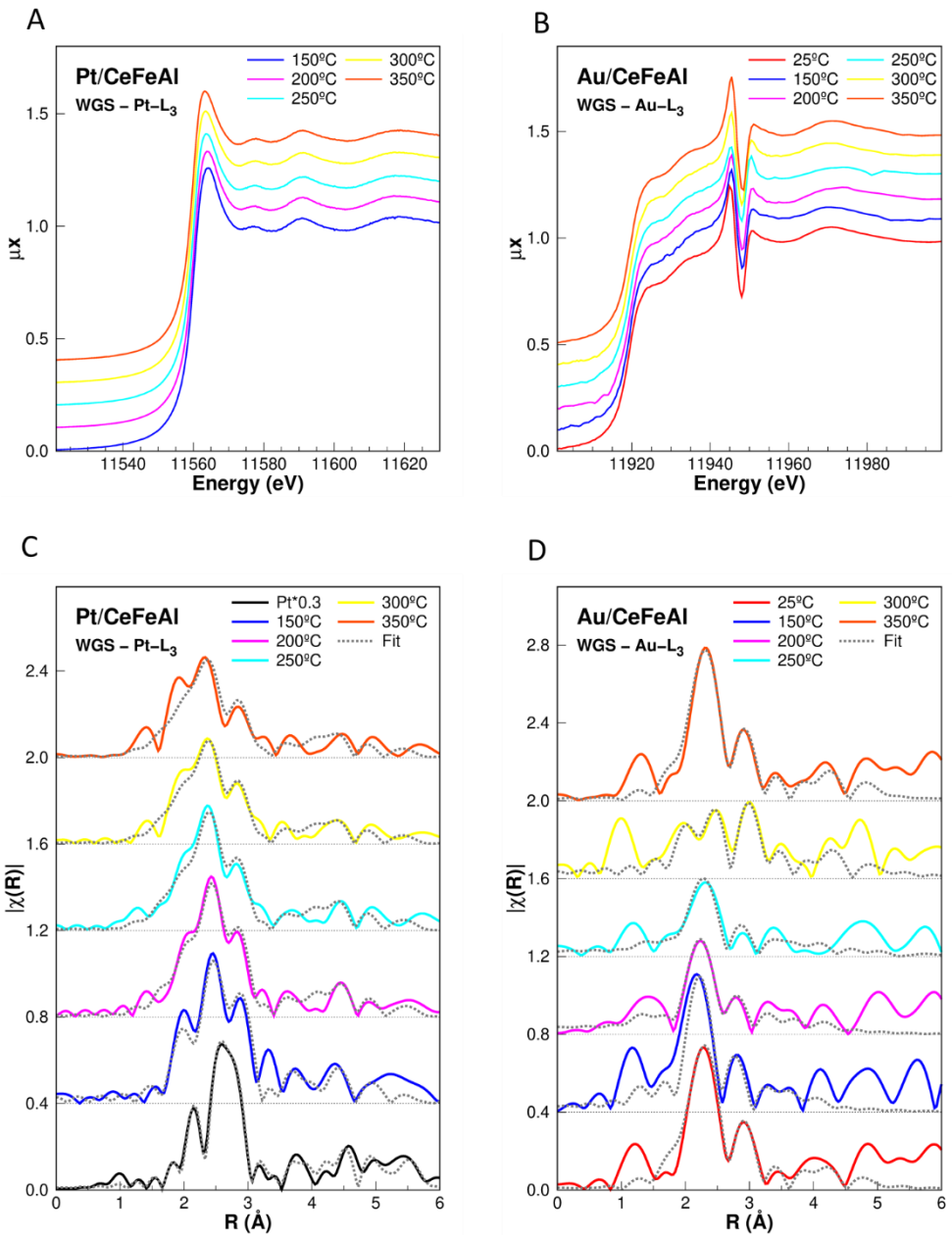

Figure 3. XAS spectra obtained during WGS reaction: A) XANES Pt-L_3; B) XANES Au-L_3; C) EXAFS Pt-L_3; D) EXAFS Au-L_3

In-situ Pt-L_3 and Au-L_3 EXAFS spectra (Fig. 3C and 3D) evidenced the different behaviors observed for Pt and Au metal. An EXAFS model was built and fitted to the experimental data by using the FEFF6 and FEFFIT 2.54 software. Detailed information of the used model can be found in the Supporting material section. In short, Pt particles were modelled assuming that Pt atoms form epitaxial squared layers growing on top of a Ce (100) surface, with different covering

proportions, in which the Pt atoms placed at the bottom occupied positions which initially should be occupied by oxygen atoms of the CeO_2 lattice. The Au atoms EXAFS spectra were fitted with a linear combination of (1) the local environment of isolated Au atoms in direct contact with the CeO_2 (100) and (110) surfaces at specific sites, and (2) Au nanoparticles, composed of the local environments of (2.1) Au bulk in regular fcc crystal structure and (2.2) Au at the surface of the nanoparticle. The proportion of each local environment in the model is given by the Au dispersion rate and the size of the nanoparticles.

Moreover, rather good fittings were obtained in the *in-situ* Pt-L_3 EXAFS spectra for Pt nanoparticles particularly at high-R providing relevant information about the Pt particle geometry. Within this region, the apparent absence of multiple-scattering signals supports the conclusion that the Pt atoms form quite small nanoparticles. Setting as starting scenario a tri-layered Pt particle, it was obtained in all the cases almost a pure bilayer, with only spurious atoms coming to the third in some cases. The Pt nanoparticle size does not exhibit meaningful variations with the temperature (**Table S6**). This may arise from the fact that the transformations are made during the previous H_2 reduction, and once the sample is in a reductive environment, it does not change significantly. In very good agreement to particle sizes observed HR-TEM micrographs (Fig. S5), the average lateral length estimated for the Pt nanoparticles is 1.2 nm, which is about 5-6 atoms per side.

Certain differences were though noticed on the shape of the Pt particle as the temperature increased from 150 to 200 °C. The intermediate layer of Pt particle showed the same size as the bottom one only at the lowest temperature (150 °C). As the temperature increased up to 200 °C, the intermediate layer became slightly larger than the bottom one. Furthermore, the coordination distances for Pt-Pt shells seem to follow a slight trend as the temperature rises, contracting the lattice at higher temperatures (**Table S7 and S8**). Being a small nanoparticle, the distances are expected to be smaller than for the bulk Pt. Such decrease on the Pt-Pt shell distances might be related to the epitaxial growth onto a slightly smaller lattice hence affecting the distances between the Pt atoms. The coordination distances for the Pt-Ce shells also experiment a transition between 150 ºC and 200 ºC (**Table S9 and S10**). At the lowest temperature, the height from the CeO_2 surface to the Pt bottom layer is 0.23 Å above the original position at the center of the tetrahedral holes. This is expected, as the Pt atom size is larger than the O_2-ions. However, this height is changed to about 0.11 at 200 ºC, and then maintained around that value at higher temperatures. This abrupt decrement on the Pt-Ce shells agrees with a Pt particle reconstruction in which an

epitaxial growth process take place from 150 °C to 200 °C coinciding with the increase on the Pt catalyst WGS rate. The Debye-Waller factors for Pt-Ce and Pt-Pt shells (**Table S8 and S10**) follow quite a regular increase as temperature rises, in accordance with the higher dynamical disorder at higher temperatures. This interesting result narrows the different models of possible shapes since it could be speculated that the nanoparticle is building the second layer larger than the first, which would be compatible with an incomplete cuboctahedral nanoparticle i.e. the preferred shape of 3D nanoparticles composed of atoms that naturally form FCC structures [32], as Pt does.

In-situ Au-L_3 EXAFS experiments are presented in Fig. 3D. From the spectra it is visualized that at the beginning of the reaction the profiles fits well with the Au bulk crystal. In other words, there is a predominance of Au-Au environment. Still, when the reaction temperature increases the shape of the oscillations dramatically change (between 200-300ºC). At these temperatures, the spectra correspond mainly to the situation in which Au is dispersed on CeO_2 surface (**Fig. S2 and Fig S3**). This means that, at the mentioned temperatures, no *Au bulk* environments are present pointing to a complete Au dispersion over the CeO_2 surface. It seems that Au nanoparticles are broken during the reaction thus achieving total dispersion on the CeO_2 surface. Nevertheless, this proportion decreases at temperatures above 250 ºC evidencing Au agglomeration. This observation is of crucial importance since it somewhat reflects the dynamics of the reaction in which a sequence of particle splitting and agglomeration for Au nanostructures is evidenced. In particular, the movements of Au particles over the CeO_2 surface are likely related to the competition of Au nanoparticles and water to be placed on the oxygen vacancies of the support which is a consequence of the double role of the support vacancies (water activation and Au particles nucleation sites). In any case, our data manifest that at a certain point of the reaction, at elevated temperatures where the activity is high, Au is completely dispersed on the CeO_2 surface in direct contact with oxygen from the support lattice. Remarkably, this contact may be explained in terms of an electrostatic Au-O interaction since Au preserves its Au^0 oxidation state during the whole process as seen in the XANES data.

The XAS Ce-L_3 spectra obtained for both catalysts under reaction conditions are shown in Fig. 4. Likewise for Pt atoms, the average oxidation state for cerium in the Pt catalyst remained almost unchanged during WGS reaction whatever the reaction temperature. For the Au based catalyst, cerium reduces under WGS reaction as the temperature increases. Once again, this different behavior may be understood considering that the Pt catalysts are H_2-reduced prior to the

WGS reaction, while the Au catalysts are not. Moreover, both catalysts achieved comparable Ce^{3+}/Ce^{4+} oxidation state ratios (around 0.45) under reaction conditions. In the analysis for the *in-situ* EXAFS Ce-L_3 spectra, CeO_2 nanoparticles were modelled assuming two different local environments (Fig. S4): atoms at the surface (external part of the nanoparticle) and atoms from the bulk (internal part of the particles). The bulk local environment was fitted by using the fluorite-type structure of CeO_2 while the external part of the nanoparticles was adjusted considering the coordination numbers and distances of the atoms at either the (100) or the (110) CeO_2 faces, because these are the most reactive faces for CeO_2 based catalysts [34]. Besides, a Ce-OH coordination shell was added to the surface Ce atoms. A linear combination of both environments was used to fit the experimental data. Both samples showed two distinct peaks depending on the R value. One at low-R, which is in fact a double peak or a peak with a shoulder that is the result of the interference between the Ce-O(1) shell of the bulk CeO_2 structure with the Ce-OH shell of the surface Ce, which should have different coordination distances. The second peak is the combination of the Ce-Ce shell with the Ce-O(2) shell. For Pt/CeFeAl sample, it was detected that the CeO_2 lattice is constrained by 0.1 Å respect to the ideal value for all the temperatures. Oppositely, in the case of the Au Au/CeFeAl sample, this contraction increased from 0.05 Å at 25 ^{o}C to 0.1 Å at higher temperatures indicating that oxygen vacancies formation happens during the reaction. This can be justified by the presence of oxygen vacancies which gives the lattice some space to collapse into itself.

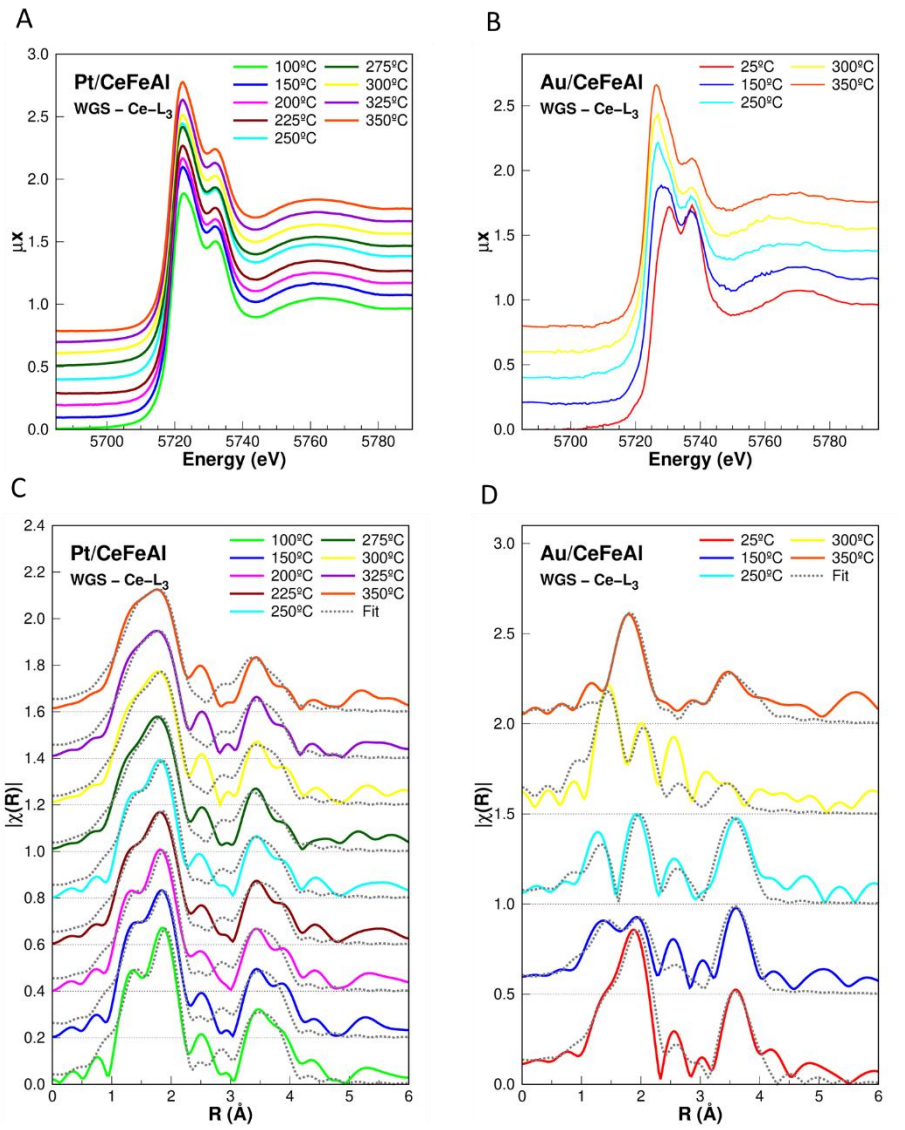

Figure 4. XAS spectra obtained during the WGS reaction for Ce-L_3 A) Pt/CeFeAl - XANES Ce-L_3; B) Au/CeFeAl - XANES Ce-L_3; C) Pt/CeFeAl - EXAFS Ce-L_3; D) Au/CeFeAl - EXAFS Ce-L_3

The EXAFS analysis of CeO_2 also permitted to estimate the proportion of *CeO_2 surface-to-CeO_2 bulk* for Au (Table 1) and Pt (**Table S5**) catalysts. The surface ratio was found strongly correlated to the Ce-OH coordination number. In the case of the Pt system, a combined value of surface to bulk ratio around 70 % and Ce-OH coordination number around 4 provided the best fits at all the temperatures. For Au/CeFeAl catalyst, relatively small (25 %) surface to bulk ratio were obtained at room temperature but it increases during the WGS reaching maximum values (68%) at relevant temperatures for the reaction (250 and 300 ºC). This value significantly decreases above

350 ºC in good agreement with the Ce^{3+}/Ce^{4+} ratio. These changes in the surface CeO_2 ratio are directly related to the Au dynamics observed in the Au-L_3 EXAFS profile (Fig. 3).

Table 1: Dispersion of Au atom on CeO_2 surface (Dispersed Au), proportion of *CeO_2 surface-to-CeO_2 bulk* (Surface Ce) as a function of the reaction temperature. Ce^{3+} percentage and CO conversion at the studied temperatures are included to underline the correlation between catalytic behavior and structural evolution during the WGS.

Temperature	Dispersed Au (%)	Surface Ce (%)	Ce^{3+} (%)	CO conversion (%)
Fresh 25º	42	-	-	0
Active 25º	43	25	0	0
WGS 150º	100	48	25	29
WGS 200º	100	-	-	61
WGS 250º	90	65	42	84
WGS 300º	45	68	51	91
WGS 350º	45	48	49	94
After 25º	45	40	35	0

The direct participation of partially reduced CeO_2 on the WGS process is also perceived on the Ce-L_3 EXAFS profile. Over partially reduced ceria, the presence of one coordination sphere at 1.2 Å (a distance too short for a Ce-O bond in the fluorite structure) accounts for the interaction of Ce and O from the H_2O (Fig.3D). For the gold ceria catalyst (not pre-reduced), this contribution appeared in a clear manner as the ceria reduced within the intermediate reaction temperatures. These data indirectly indicate that water splitting is happening on CeO_2 as well established in previous reports [11] and accounts for the different behavior exhibited by both metal supported catalysts as a function of the support nature. Indeed, a major difference between both metal relates to the water splitting process: Pt metal actively dissociates water molecules whilst the energy barrier for the water activation on Au nanoparticles is too high [17]. Therefore Au needs to be assisted by the support to complete the WGS cycle. As summarized in **Table S11,** the Ce-O distance on the surface are quite smaller compared to that observed in the bulk (2.06 *vs* 2.34 Å average distances). Actually, this coordination sphere corresponds to the interaction between Ce atoms and dissociatively adsorbed water as a consequence of the WGS reaction. According to Molinari *et al.* [35] studies, the adsorption of water on the oxygen vacancies in the CeO_2 surface leads to a dissociation of this molecule producing two hydroxyl species with the aid of a neighbor surface oxygen. The formed hydroxyl groups substitute the original surface oxygen. This hypothesis of surface hydroxylation agrees with the observed CeO_2 reduction in the XANES experiments.

For the Au catalyst, the Ce-O (oxygen from water) coordination sphere also has a particular dynamic (at 150 ºC is a shoulder, at 250 ºC is well defined and at superior temperatures disappears) manifesting water migration from CeO_2 vacancies due to Au and water competition to be placed on these punctual defects. The breakdown of Au clusters into highly dispersed Au atoms nucleating in oxygen vacancies present over partially reduced CeO_2 (schematized in Fig. 5) showcases a dynamic relation between Au and CeO_2 as both species operate together to constitute the active phase of an efficient WGS catalyst.

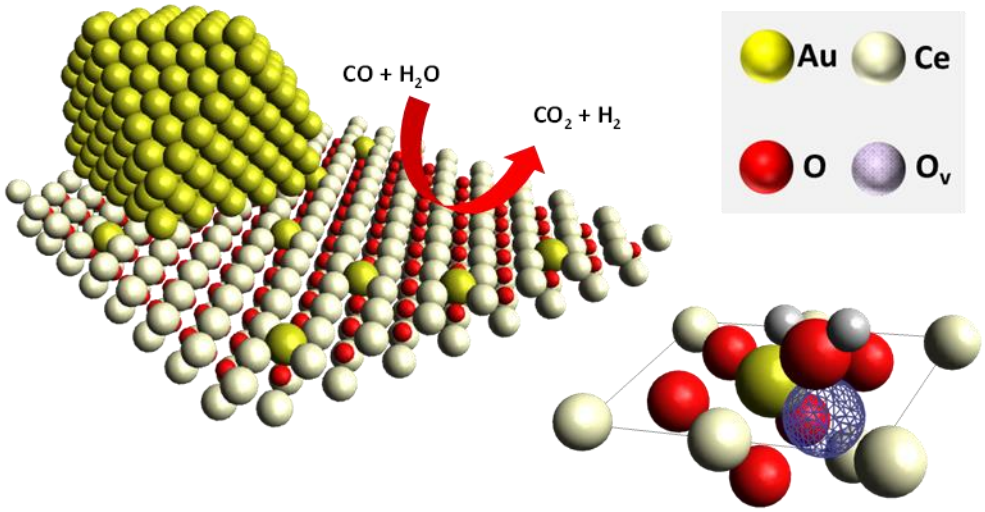

Fig. 5: Schematic representation of the WGS over the Fe doped $Au/CeO_2/Al_2O_3$ catalyst.

CONCLUSIONS

Operando X-ray absorption data of $NM/CeO_2/Al_2O_3$ catalysts enabled establishing the differences in the metal dynamics and identify the Au and Pt active sites for WGS reaction conditions. Aside of the differences attributable to the H_2 pre-treatment conducted over Pt catalyst, both Pt and Au catalysts evidence comparable reduction behavior along with the existence of a coordination sphere at ~2 Å that corresponds to the interaction of hydroxyl or water groups with partially reduced CeO_2 surfaces. This behavior is consistent with the average oxidation state of cerium estimated from the XANES spectra indicating that water desorption/splitting is favored over CeO_2 oxygen vacancies.

For the reduced Pt catalysts, the absence of changes in the Pt oxidation state points to metal Pt^0 atoms as the main WGS active sites. With respect to the Pt structural dynamics, rather constant particle sizes were maintained, and the Pt particles could growth epitaxially under WGS

atmospheres. At 200-250 ºC, and coinciding with an important increment in the achieved CO conversions, the variations noticed on the relative sizes of the intermediate and the bottom layers of the Pt particles suggested a re-structuration of the Pt atoms into cuboctahedrical particles in which the intermediate layer is composed by more atoms than the bottom one. The re-arrangement of the Pt atoms into cuboctahedrical particles involved a concomitant shortening on the Pt-Ce distances.

Concerning the Au dynamics, the proportion of Au surface atom respect to that of Au bulk increases significantly when the temperature rises up from 25 ºC to 100 ºC suggesting a complete Au redispersion. That total Au redispersion was accompanied with an increment of the Au-Ce and Au-O signals, implying that Au atoms are located close to the oxygen vacancies. Considering that the water activation steps procced on the oxygen vacancies, a Au-CeO_2 interface is key to overcome this rate-limiting step. We have demonstrated that metallic Au atoms placed close to the oxygen vacancies, being surrounded by oxygen atoms. The absence of a white line and adsorption energy shifts noticed for Au catalyst suggest that the Au-O contact is an electrostatic interaction pointing out Au^0 species as the chief active phase for the WGS reaction. Hence, the active gold species remains unoxidized while surrounded by oxygen, closing the debate in the literature about the oxidized/metallic gold as the active WGS phase.

SUPPORTING INFORMATION

Physicochemical characterization of catalysts, detailed description of XAS model approach and tables with obtained fitting parameters.

ACKNOWLEDGEMENTS

We acknowledge ALBA and SOLEIL synchrotrons, and the NSLS at Brookhaven National Laboratory (BNL) for provision of synchrotron radiation facilities and for beamtime allocation. The research carried out at BNL was supported under contract DE-SC0012704 with the US Department of Energy, Division of Chemical Sciences. We would like to thank C. Marini and the rest of CLÆSS, SAMBA, and X18B beamlines scientific and technical staff for their invaluable help during the beamtime. Authors would also like to acknowledge Spanish Ministry of Science and Innovation through the projects (RTI2018-096294-B-C33) and RYC2018-024387-I.

REFERENCES

(1) Song, C. Fuel Processing for Low-Temperature and High-Temperature Fuel Cells: Challenges, and Opportunities for Sustainable Development in the 21st Century. *Catal. Today* **2002**, *77* (1–2), 17–49. https://doi.org/10.1016/S0920-5861(02)00231-6.

(2) Trimm, D. L. Minimisation of Carbon Monoxide in a Hydrogen Stream for Fuel Cell Application. *Appl. Catal. A Gen.* **2005**, *296* (1), 1–11. https://doi.org/10.1016/j.apcata.2005.07.011.

(3) Farrauto, R.; Liu, Y.; Ruettinger, W.; Ilinich, O.; Shore, L.; Giroux, T. Precious Metal Catalysts Supported on Ceramic and Metal Monolithic Structures for the Hydrogen Economy. *Catal. Rev. - Sci. Eng.* **2007**, *49* (2), 141–196. https://doi.org/10.1080/01614940701220496.

(4) Petallidou, K. C.; Kalamaras, C. M.; Efstathiou, A. M. The Effect of La 3 + , Ti 4 + and Zr 4 + Dopants on the Mechanism of WGS on Ceria-Doped Supported Pt Catalysts. *Catal. Today* **2014**, *228*, 183–193. https://doi.org/10.1016/j.cattod.2013.10.081.

(5) Farrauto, R. J. New Catalysts and Reactor Designs for the Hydrogen Economy. *Chem. Eng. J.* **2014**, *238*, 172–177. https://doi.org/10.1016/j.cej.2013.07.004.

(6) Park, J. B.; Graciani, J.; Evans, J.; Stacchiola, D.; Senanayake, S. D.; Barrio, L.; Liu, P.; Sanz, J. F.; Hrbek, J.; Rodriguez, J. A. Gold, Copper, and Platinum Nanoparticles Dispersed on CeO x/TiO2(110) Surfaces: High Water-Gas Shift Activity and the Nature of the Mixed-Metal Oxide at the Nanometer Level. *J. Am. Chem. Soc.* **2010**, *132* (1), 356–363. https://doi.org/10.1021/ja9087677.

(7) Andreeva D., Idakiev V., Tabakova T., Ilieva L., Falaras P., Bourlinos A., Travlos A. Low-temperature water-gas shift reaction over Au/CeO_2 catalysts. Catal Today **2002**, *72*, 51-57. https://doi.org/10.1016/S0920-5861(01)00477-1

(8) González-Castaño, M.; Reina, T. R.; Ivanova, S.; Martínez Tejada, L. M.; Centeno, M. A.; Odriozola, J. A. O2-Assisted Water Gas Shift Reaction over Structured Au and Pt Catalysts. *Appl. Catal. B Environ.* **2016**, *185*, 337–343. https://doi.org/10.1016/j.apcatb.2015.12.032.

(9) Daly, H.; Goguet, A.; Hardacre, C.; Meunier, F. C.; Pilasombat, R.; Thompsett, D. The Effect of Reaction Conditions on the Stability of Au/CeZrO4 Catalysts in the Low-Temperature Water-Gas Shift Reaction. *J. Catal.* **2010**, *273* (2), 257–265. https://doi.org/10.1016/j.jcat.2010.05.021.

(10) Rodriguez, J. A.; Ma, S.; Liu, P.; Hrbek, J.; Evans, J.; Pérez, M. Activity of CeOx and

TiOx Nanoparticles Grown on Au(111) in the Water-Gas Shift Reaction. *Science (80-.).* **2007**, *318* (December), 1757–1760.

(11) Bonda, G.; Thompson, D. Formulation of Mechanisms for Gold-Catalysed Reactions. *Gold Bull.* **2009**, *42* (4), 247–259.

(12) Ratnasamy, C.; Wagner, J. Water Gas Shift Catalysis. *Catal. Rev. - Sci. Eng.* **2009**, *51* (3), 325–440. https://doi.org/10.1080/01614940903048661.

(13) Jacobs, G.; Davis, B. H. Low Temperature Water-Gas Shift: Applications of a Modified SSITKA-DRIFTS Method under Conditions of H2 Co-Feeding over Metal/Ceria and Related Oxides. *Appl. Catal. A Gen.* **2007**, *333* (2), 192–201. https://doi.org/10.1016/j.apcata.2007.07.029.

(14) Fu, Q.; Saltsburg, H.; Flytzani-Stephanopoulos, M. Active Nonmetallic Au and Pt Species on Ceria-Based Water-Gas Shift Catalysts. *Science (80-.).* **2003**, *301* (5635), 935–938. https://doi.org/10.1126/science.1085721.

(15) Yang, M.; Li, S.; Wang, Y.; Herron, J. A.; Xu, Y.; Allard, L. F.; Lee, S.; Huang, J.; Flytzani-stephanopoulos, M. Catalytically Active Au-O (OH) - Species Stabilized by Alkali Ions on Zeolites and Mesoporous Oxides. **2014**, *346* 6216 1498-1501

(16) Li, Y.; Kottwitz, M.; Vincent, J. L.; Enright, M. J.; Liu, Z.; Zhang, L.; Huang, J.; Senanayake, S. D.; Yang, W. C. D.; Crozier, P. A.; Nuzzo, R. G.; Frenkel, A. I. Dynamic Structure of Active Sites in Ceria-Supported Pt Catalysts for the Water Gas Shift Reaction. *Nat. Commun.* **2021**, *12* (1), 1–9. https://doi.org/10.1038/s41467-021-21132-4.

(17) Gonzalez Castaño, M.; Reina, T. R.; Ivanova, S.; Centeno, M. A.; Odriozola, J. A. Pt vs. Au in Water–Gas Shift Reaction. *J. Catal.* **2014**, *314*, 1–9. https://doi.org/10.1016/j.jcat.2014.03.014.

(18) Kalamaras, C. M.; Dionysiou, D. D.; Efstathiou, A. M. Mechanistic Studies of the Water-Gas Shift Reaction over Pt/Ce XZr1-XO2 Catalysts: The Effect of Pt Particle Size and Zr Dopant. *ACS Catal.* **2012**, *2* (12), 2729–2742. https://doi.org/10.1021/cs3006204.

(19) Kim, C. H.; Thompson, L. T. On the Importance of Nanocrystalline Gold for Au/CeO2 Water-Gas Shift Catalysts. *J. Catal.* **2006**, *244* (2), 248–250. https://doi.org/10.1016/j.jcat.2006.08.018.

(20) Karpenko, A.; Leppelt, R.; Plzak, V.; Behm, R. J. The Role of Cationic Au3+ and Nonionic Au0 Species in the Low-Temperature Water-Gas Shift Reaction on Au/CeO2 Catalysts. *J. Catal.* **2007**, *252* (2), 231–242. https://doi.org/10.1016/j.jcat.2007.09.017.

(21) Liu, P.; Rodriguez, J. A. Water-Gas-Shift Reaction on Metal Nanoparticles and Surfaces. *J. Chem. Phys.* **2007**, *126* (16). https://doi.org/10.1063/1.2722747.

(22) González, I. D.; Navarro, R. M.; Wen, W.; Marinkovic, N.; Rodriguéz, J. A.; Rosa, F.; Fierro, J. L. G. A Comparative Study of the Water Gas Shift Reaction over Platinum Catalysts Supported on CeO2, TiO2 and Ce-Modified TiO2. *Catal. Today* **2010**, *149* (3–4), 372–379. https://doi.org/10.1016/j.cattod.2009.07.100.

(23) Ding, K.; Gulec, A.; Johnson, A. M.; Schweitzer, N. M.; Stucky, G. D.; Marks, L. D.; Stair, P. C. Identification of Active Sites in CO Oxidation and Water-Gas Shift over Supported Pt Catalysts. *Science (80-.).* **2015**, *350* (6257), 189–192. https://doi.org/10.1126/science.aac6368.

(24) Gonzalez Castaño, M.; Reina, T. R. R.; Ivanova, S.; Centeno, M. a. A.; Odriozola, J. a. A. Pt vs. Au in Water-Gas Shift Reaction. *J. Catal.* **2014**, *314*, 1–9. https://doi.org/10.1016/j.jcat.2014.03.014.

(25) Romero-Sarria, F.; Garcia-Dali, S.; Palma, S.; Jimenez-Barrera, E. M.; Oliviero, L.; Bazin, P.; Odriozola, J. A. The Role of Carbon Overlayers on Pt-Based Catalysts for H2-Cleanup by CO-PROX. *Surf. Sci.* **2016**, *648*, 84–91. https://doi.org/10.1016/j.susc.2015.12.017.

(26) Reina, T. R.; Ivanova, S.; Delgado, J. J.; Ivanov, I.; Idakiev, V.; Tabakova, T.; Centeno, M. A.; Odriozola, J. A. Viability of Au/CeO2-ZnO/Al2O3 Catalysts for Pure Hidrogen Production via WGS. *ChemCatChem* **2014**, *6*, 1401–1409. https://doi.org/10.1002/cctc.200)).

(27) González-Castaño, M.; Ivanova, S.; Laguna, O. H.; Martínez T., L. M.; Centeno, M. A.; Odriozola, J. A. Structuring Pt/CeO2/Al2O3 WGS Catalyst: Introduction of Buffer Layer. *Appl. Catal. B Environ.* **2017**, *200*, 420–427. https://doi.org/10.1016/j.apcatb.2016.07.039.

(28) Hernández, W. Y.; Romero-Sarria, F.; Centeno, M. A.; Odriozola, J. A. In Situ Characterization of the Dynamic Gold-Support Interaction over Ceria ModifiedEu3+. Influence of the Oxygen Vacancies on the Co Oxidation Reaction. *J. Phys. Chem. C* **2010**, *114* (24), 10857–10865. https://doi.org/10.1021/jp1013225.

(29) Bobadilla, L. F.; Santos, J. L.; Ivanova, S.; Odriozola, J. A.; Urakawa, A. Unravelling the Role of Oxygen Vacancies in the Mechanism of the Reverse Water − Gas Shift Reaction by Operando DRIFTS and Ultraviolet − Visible Spectroscopy. ACS Catal. **2018,** 8, 7455−7467. https://doi.org/10.1021/acscatal.8b02121.

(30) Bera, P.; Priolkar, K. R.; Gayen, A.; Sarode, P. R.; Hegde, M. S.; Emura, S.; Kumashiro,

R.; Jayaram, V.; Subbanna, G. N. Ionic Dispersion of Pt over CeO2 by the Combustion Method: Structural Investigation by XRD, TEM, XPS, and EXAFS. *Chem. Mater.* **2003**, *15* (10), 2049–2060. https://doi.org/10.1021/cm0204775.

(31) Linganiso, L. Z.; Pendyala, V. R. R.; Jacobs, G.; Davis, B. H.; Cronauer, D. C.; Kropf, A. J.; Marshall, C. L. Low-Temperature Water-Gas Shift: Doping Ceria Improves Reducibility and Mobility of o-Bound Species and Catalyst Activity. *Catal. Letters* **2011**, *141* (12), 1723–1731. https://doi.org/10.1007/s10562-011-0720-1.

(32) Barrabés, N.; Föttinger, K.; Llorca, J.; Dafinov, A.; Medina, F.; Sá, J.; Hardacre, C.; Rupprechter, G. Pretreatment Effect on Pt/CeO 2 Catalyst in the Selective Hydrodechlorination of Trichloroethylene. *J. Phys. Chem. C* **2010**, *114* (41), 17675–17682. https://doi.org/10.1021/jp1048748.

(33) López-Cartes, C.; Rojas, T. C.; Litrán, R.; Martínez-Martínez, D.; De La Fuente, J. M.; Penadés, S.; Fernández, A. Gold Nanoparticles with Different Capping Systems: An Electronic and Structural XAS Analysis. *J. Phys. Chem. B* **2005**, *109* (18), 8761–8766. https://doi.org/10.1021/jp050184+.

(34) Sayle, D. C.; Maicaneanu, S. A.; Watson, G. W. Atomistic Models for CeO2(111), (110), and (100) Nanoparticles, Supported on Yttrium-Stabilized Zirconia. J. Am. Chem. Soc. **2002**, 124, 38, 11429–11439

(35) Molinari, M.; Parker, S. C.; Sayle, D. C.; Islam, M. S. Water Adsorption and Its Effect on the Stability of Low Index Stoichiometric and Reduced Surfaces of Ceria. *J. Phys. Chem. C* **2012**, *116*, 7073–7082.

TOC Graphic